Constrained Multi-Objective Wind Farm Layout Optimization: Novel Constraint Handling Approach Based on Constraint Programming

Sami Yamani Douzi Sorkhabi[a,*], David A. Romero[b], J. Christopher Beck[b], Cristina H. Amon[b]

[a] *Department of Mechanical Engineering, Massachusetts Institute of Technology, Cambridge, MA, USA.*

[b] *Department of Mechanical & Industrial Engineering, University of Toronto, Toronto, ON, Canada.*

Abstract

Wind farms are frequently located in proximity to human dwellings, natural habitats, and infrastructure making land use constraints and noise matters of increasing concern for all stakeholders. In this study, we perform a constrained multi-objective wind farm layout optimization considering energy and noise as objective functions, and considering land use constraints arising from landowner participation, environmental setbacks and proximity to existing infrastructure. A multi-objective, continuous variable Genetic Algorithm (NSGA-II) is combined with a novel constraint handling approach to solve the optimization problem. This constraint handling approach uses a combination of penalty functions and Constraint Programming to balance local and global exploration to find feasible solutions. The proposed approach is used to solve the wind farm layout optimization problem with different numbers of turbines and under different levels of land availability (constraint severity). Our results show increasing land availability and/or number of turbines, increases energy generation, noise production, and computational cost. Results also illustrate the potential of the proposed constraint handling approach to outperform existing methods in the context of evolutionary optimization, yielding better solutions at a lower computational cost.

Keywords: Wind farm layout, multi-objective optimization, Constraint Programming, penalty functions.

*Corresponding author

Email address: syamani@mit.edu (Sami Yamani Douzi Sorkhabi)

Nomenclature

Roman Symbols

$\mathbb{R}$	Set of coordinates of noise receptors
$\mathbb{T}$	Set of coordinates of turbines
$\mathcal{D}$	Set of all direction-speed wind states
a	Turbine induction factor
A_f	Octave-band A-weighting correction, dB
A_P	Non-feasible polygon area, m^2
A_w	Octave-band noise attenuation, dB
c	Constraint
C_T	Thrust coefficient of the turbine
D	Diameter of turbine rotor, m
d	Distance between a turbine that violates a constraint and the closest feasible region
f	Objective function
g	Amount of constraint violation
l	Number of variables
L_W	Turbine sound power emittance, dB
m	Number of constraints
n	Number of objective functions
n_T	Number of turbines
n_{gen}	Total number of generations
n_{nf}	Number of infeasible turbines
n_{reg}	Number of turbines violating regulatory constraints
p_d	Wind state probability
r_r	Radius of turbine rotor, m
R_{AEP}	Penalty coefficient for energy objective function
R_{SPL}	Penalty coefficient for sound objective function
t	Current generation index

u Downstream wind speed, m/s

u_0 Upstream wind speed, m/s

u_a Wind speed behind turbine rotor, m/s

Acronyms

AEP^P Penalized annual energy production objective function

SPL^P Penalized sound pressure level objective function

AEP Annual Energy Production

CHCP Constraint Handling via Constraint Programming

CP Constraint Programming

GA Genetic Algorithm

MD Maximum Distance

MIP Mixed Integer Programming

NSGA-II Non-dominated Sorting Genetic Algorithm-II

SPL Sound Pressure Level

WFLO Wind Farm Layout Optimization

Greek Symbols

α Turbine entrainment factor

ϕ Domain feasibility percentage

1. Introduction

Installed capacity for generating electricity from wind has seen a significant increase during the past decade [1–3]. In contrast to these growing trends, wind energy still faces resistance to being widely used onshore, due to health and environmental concerns. Although it is not proven that the noise production of turbines can have negative health impact, a number of jurisdictions have established regulations that limit noise emissions [4–6].

Wind farm design can be an iterative, lengthy process, in which designers have to check for compliance with land use constraints and environmental restrictions. Traditionally wind farm designers and researchers have considered energy or profit as the objective functions to be maximized [7, 8], while some included other constraints such as land use, setbacks, noise limits, and terrain complexity in their optimization model [9–14]. Among these constraints, however, noise production of turbines has been considered as an objective function together with energy generation, making the problem a multi-objective optimization [15–17]. This consideration elucidates the nature of trade-off between energy generation and noise production as highly dependent characteristics of wind farms. With the goal of further exploring this trade-off and proposing a more efficient optimization approach, the focus of this study is on multi-objective optimization considering energy generation and noise production as objective functions, while taking land use constraints into account.

Stochastic metaheuristics such as Genteic Algorithms (GAs) [18] and Particle Swarm Optimization (PSO) [19] are the most common approaches for the wind farm layout optimization problem [7, 8, 20, 21]. In addition, deterministic heuristics such as the Extended Pattern Search (EPS) approach of Du Pont and Cagan [22] are also used. Donovan [23, 24] and Fagerfjäll [25] introduced an alternative approach which uses mixed-integer programming (MIP) and solves the wind farm layout optimization (WFLO) problem by the traditional branch-and-bound method. Although MIP solvers are widely available in operation research software packages, they all have limitations solving non-linear, non-convex problems such as WFLO. Thus, Donovan and Fagerfjäll made some approximations in their wake models and simplified the problem at the expense of accuracy in the solutions. Archer et al. [26] improved the accuracy of the simplified wake model by introducing a wind interference coefficient, while Turner et al. [27] suggested more accurate linear and quadratic mathematical optimization models that can be solved by MIP solvers. The accuracy problem was resolved by Zhang et al. [17], who proposed the first Constraint Programming (CP) and MIP models that incorporated the full non-linearity of the problem. Despite these advances in the solution of the WFLO with mathematical programming models, all of them use a discretized domain to solve the problem, a feature that can lead to suboptimal solutions. Moreover, these state-of-the-art MIP models [17, 27] still suffer from limitations on problem size and turbine density, e.g., typically discretizing the wind farm into only $100 - 400$ potential turbine locations. To address the limitations associated with mathematical programming, Guirguis et al. [28] recently proposed a continuous-variable, gradient-based, non-linear optimization approach that relies on exact gradient information to solve the WFLO problem. The authors showed that this approach outperforms the current mathematical programming approaches.

One challenge to the use of stochastic algorithms to solve multi-objective optimization problems is a technique to ensure feasible solutions. Typically, stochastic algorithms search through both feasible and infeasible space, with the possibility that the lowest cost solution found will fail to satisfy some hard constraints. Penalty functions are the most widely used approach to bias evolutionary algorithms toward feasible solutions due to their simplicity, applicability, and strong theoretical basis [29]. This approach adds a function of constraint violations to the objective functions recasting the constrained problem as unconstrained. Thus, penalty functions can be used for constraint handling, regardless of the optimization method that solves the recast unconstrained optimization problem. When penalty functions are used with evolutionary algorithms, there is no need for an initial feasible population, which is by itself NP-hard to compute for many problems.

However, the penalty function approach has several limitations. When a penalty function penalizes the objective functions of a solution, it is unlikely for that solution to pass through to the next generation. As a result, the penalty function approach favors global exploration when dealing with infeasible solutions, potentially slowing convergence when the solution lies on the feasibility boundary. Although previous research works (e.g., [30]) have tried to address this issue, none of them have suggested what we term *local exploration*: an approach to generate new feasible solutions in the neighborhood of the current infeasible solution. In contrast, we use the term *global exploration* to refer to the search for new solutions elsewhere in the search space. With these definitions, our goals in this work are to improve the ability to solve continuous, multi-objective WFLO problems through enhancement of the penalty function approach with an efficient local exploration approach.

Other approaches based on multi-stage optimization or adaptive operators have been used for constraint handling with evolutionary algorithms, with the most recent of these approaches proposed by Elsayed et al. [31]. At each generation, multiple search operators are used and the appropriate combination of these search operators is determined adaptively. Oh et al. [32] also suggested a general constraint handling approach in which the subset of constraints that plays a key role in feasibility within a certain tolerance is selected and handled before the other constraints. This tolerance is specified by statistics on feasible solutions and several predefined criteria. The selected constraints are handled first to guide the solution set toward the feasible region. Constrained multi-objective optimization problems can also be tackled based on constrained-domination [33]. In these methods, an extended Pareto dominance criterion considers constraint violations as a second-tier dominance check, potentially demoting infeasible solutions to a lower non-domination rank [34]. A more comprehensive approach for constraint-domination [35] ranks the solutions based on their objective function values, constraint violations, and a combination of objective function values and constraint violations. A recent study by Jain et al. [36] uses Deb's constraint-domination approach [34] together with a reference-point based non-domination sorting. Mohamed et al. [37] modified Deb's constraint handling approach to consider the sum of constraint violation as a second metric to handle the constraints. All the aforementioned approaches have had an acceptable performance when applied to different benchmark or engineering problems; however, they are all based on biasing the search towards the feasible region by discarding infeasible solutions.

Some previous studies have employed Constraint Programming (CP) to improve the performance of evolutionary optimization algorithms. In a study by Wang et al. [38] a CP-based GA is developed to solve the resource portfolio planning of make-to-stock products problem. They formulated the problem as a non-linear mixed integer programming (MIP) and solved it using GA. The infeasible solutions that are generated in the recombination process of the GA are repaired by the CP model that finds a feasible solution in proximity with the infeasible solution in the objective space. In a recent study by Di Alesio et al. [39] GA and CP are combined to support stress testing of task deadlines. After each generation, the GA passes the new generation to the CP model, which modifies the solutions, while considering the constraints. Zhu et al. [40] proposed a combination of GA and boolean CP for solving course of action optimization in Influence Nets. One aspect of algorithm behavior that these studies failed to analyze is the extent to which the CP search reduces the diversity of the population. In other words, it is not clear the extent to which local exploration of CP prevents the optimization algorithm from performing global exploration. Thus, it is necessary to investigate the potential of using an alternative global exploration constraint handling approach as a complement for CP.

In this study, a novel approach is proposed for constrained multi-objective, continuous problems, by hybridizing Constraint Programming and penalty functions for constraint handling. The proposed approach solves the optimization problem with the NSGA-II algorithm, launching sub-problems to repair infeasible solutions given a strict computational budget. Infeasible solutions that could not be repaired with the given computation budget are handled by standard dynamic penalty operators. By leveraging Constraint Programming methods as a constraint handling operator within Evolutionary Algorithms, we perform a combination of global exploration and local exploitation and improve the efficiency of the optimization algorithm without adding to the computational cost.

The proposed approach is used for wind farm layout optimization under land-use constraints. The WFLO problem is formulated to consider energy generation (maximize), noise levels (minimize), and compliance with land-use and setback constraints, extending previous work of Kwong et al. [15, 16]. Results show that the convergence rate for the proposed CP/Penalty hybrid outperformed that of the Penalty-only approach within the same run-time. In the context of the WFLO problem, results show that in the most constrained case studied in this work, annual energy production is increased by 50 MWh and average noise received by noise receptors is reduced by 0.42 dBA compared to solutions found by handling optimization constraints with penalty operators only.

2. Constrained WFLO Problem Formulation

In this problem, the goal is to maximize the energy generation of a wind farm, while minimizing the noise levels estimated at any residence inside the wind farm or in its neighborhood.

In order to calculate energy generation of the wind farm, changes in the wind speed due to the interaction of multiple wake regions needs to be understood. This understanding can provide us with the wind speed profile inside the wind farm. Finally, Annual Energy Production (AEP) of wind farm can be calculated based on wind speed profile and power generation of turbines.

To calculate wind speed inside a single wake region, Jensen's wake model [41] is used. The key assumption in this model is that the wake area immediately behind the turbine rotor is equal to the sweeping area of the turbine. Based on the mass conservation principle, and assuming a linear expansion of the wake profile, the wind speed (u) at an arbitrary distance (x) downstream of the turbine can be written as,

$$u = u_0 \left(1 - a \frac{r_r^2}{(r_r + \alpha x)^2} \right), \tag{1}$$

where u_0 is the upstream wind speed, r_r is the radius of the turbine, a is the turbine induction factor, and α is the turbine entrainment factor calculated using the following empirical correlation,

$$\alpha = \frac{0.5}{\ln \frac{Z}{Z_0}}, \tag{2}$$

where Z is the turbine hub height and Z_0 is terrain roughness. In Equation 1, turbine induction factor is defined as,

$$a = 1 - \frac{u_a}{u_0} \tag{3}$$

where u_a is the wind speed immediately after turbine rotor. Jensen [41] correlated the turbine induction factor (a) to the thrust coefficient of turbine (C_T) as,

$$C_T = 4a(1 - a) \tag{4}$$

where C_T is often provided by turbine manufacturer.

The above analysis is valid for a single wake region only. To take the effect of multiple wake interactions into account, a commonly used approach [42–44] is to assume that the total kinetic energy deficit at a any location inside the wind farm is the sum of the kinetic energy deficits caused by each single wake affecting that location. Mathematically, the wind speed at an arbitrary location i that is affected by the wake region of k upstream turbines can be calculated as,

$$(u_0 - u_i)^2 = \sum_{j=1}^{k} \left((u_0 - u_{ij})\right)^2, \tag{5}$$

where u_{ij} is the wind speed at location i if this location was only affected by the wake region of turbine j. The value of u_{ij} can be determined using Eq. 1. In this work, we have used the kinetic energy deficit approach for wake combination (Eq. 5) and Jensen's wake model (Eqns. 1, 2, 3, and 4) to estimate the wind speed profile at any point inside the wind farm. The rational behind this modelling choice, besides its wide adoption in the relevant literature, is that WFLO is concerned with mid- and far-wake behavior, while more detailed (and mathematically complex) models of wind turbines provide more information about near-wake behavior. Hence, despite the limiting assumptions (flat terrain, uniform thrust, infinite number of blades, among others) to which this modelling approach owes its mathematical simplicity, it has been widely used in the literature on wind farm layout optimization (e.g., [13, 16, 45, 46]), and it has been reported to be reasonably accurate [47, 48].

In addition to wind speed profile, turbine characteristics together with the meteorological wind speed data are needed to calculate AEP. Tables 1 and 2 show turbine characteristics and power generation respectively. For the wind resource, this work implements the distribution defined by Kusiak et al. [49], which utilizes 24 wind directions in 15° intervals and 43 wind speeds from 4 m/s to 25 m/s in 0.5 m/s intervals. Each direction-speed is assigned a probability and Fig. 1 shows the distribution of these direction-speed probabilities. Based on this information, AEP can be calculated as,

$$AEP(\mathbb{T}) = \sum_{i=1}^{n_T} \sum_{d \in \mathcal{D}} P_{i,d}\, p_d, \tag{6}$$

where $\mathbb{T}$ is the set of turbine coordinates, n_T is the number of turbines, $\mathcal{D}$ is the set of wind states, $P_{i,d}$ is the power generation of turbine i at wind state d, and p_d is the annual probability of wind state d (i.e. wind speed and direction).

In wind farm layout design, all residences inside or in the neighbourhood of wind farm are potential noise receptors and sound level needs to be measured at them. Following the previous work [15, 16, 46, 50, 51], we use ISO-9613-2 standard [52],

Table 1: Wind turbine parameters.

Parameter	Value
Turbine Hub Height (Z)	80 m
Terrain Roughness Length (Z_0)	0.1 m
Rotor Radius (r_r)	38.5 m
Thrust Coefficient (C_T)	0.8
Cut-in Speed	4 m/s
Cut-off Speed	25 m/s
Rated Speed	15 m/s
Rated Power	1.5 MW
Average Noise Production (L_w)	100 dB

Table 2: Power output of a single turbine as a function of wind speed.

Wind Speed (m/s)	4	5	6	7	8	9
P (kW)	63.44	204.30	345.16	486.02	626.88	767.74
Wind Speed (m/s)	10	11	12	13	14	15-25
P (kW)	908.60	1049.46	1190.32	1331.18	1472.04	1500.00

to calculate the equivalent continuous downwind octave-band sound pressure level (SPL) at each noise receptor and for each sound source. The countinous audiable frequency range is discretized to eight octave bands with nominal mid-band frequencies from 63 Hz to 8 kHz and SPL for each octave-band (L_f) can be written as $L_f = L_W - A_w(f)$, where L_W is the octave-band sound power emitted by the source, and $A_w(f)$ is the octave-band attenuation. Table 3 shows the values of L_W for the studied turbine at different wind speeds. The attenuation term, i.e., $A_w(f)$, is the sum of attenuation effects caused by geometrical divergence, atmospheric absorption, ground effects, sound barriers, and miscellaneous effects. In the present work, we followed the previous work by assuming negligible attenuation effects due to sound barriers and miscellaneous effects. The readers are referred to [52] for comprehensive details on how to calculte attenuation term. Sine the hearing system of human is more sensative to certain frequencies, the SPL calculated for each octave-band has to be converted to an effective SPL. Among several octave-band weightings available for this conversion, A-weighted sound pressure levels [6] are customarily used in wind

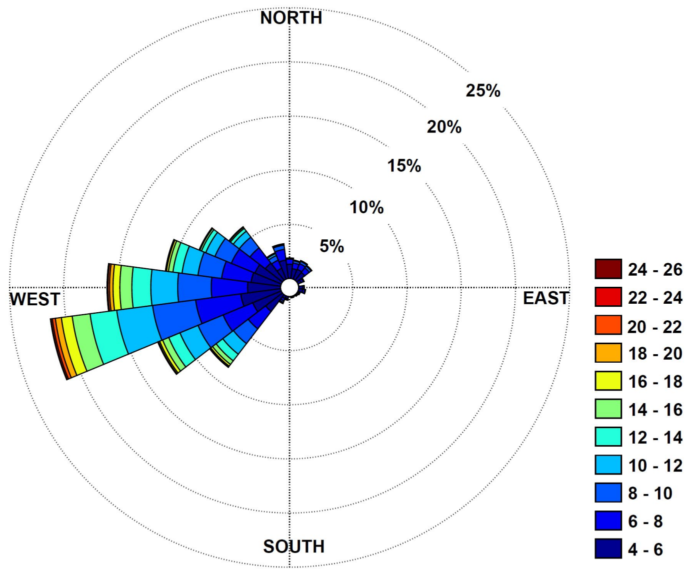

Figure 1: Wind rose showing the distribution of speed-direction probabilities.

Table 3: Sound power emittance (L_W) of turbine at different wind speeds.

Wind Speed (m/s)	3	7.2	7.9	8.6	9.3	10	11.5	12.9	25
$\mathbf{L_W}$ **(dB)**	97.1	97.1	99.7	102.0	103.4	104.0	104.0	104.0	104.0

farm layout design. The equivalent continuous A-weighted downwind sound pressure level at a specific location is calculated as,

$$SPL(\mathbb{T},\mathbb{R}) = 10\log\left(\sum_{i=1}^{n_T}\sum_{j=1}^{8} 10^{0.1\left(L_f^{(i,j)}(\mathbb{T},\mathbb{R})+A_f^{(j)}\right)}\right), \tag{7}$$

where $\mathbb{R}$ is the set of noise receptor coordinates. Further details for the calculation procedure are available in the ISO-9613-2 document [52].

Two constraints are considered for this problem, namely proximity and regulatory constraints. The proximity constraint restricts the distance between each pair of turbines to be at least five times their rotor diameter. This constraint is handled by calculating the Euclidean distance of turbines from each other in Cartesian coordinates. Thus, turbine i with coordinates (x_{t_i}, y_{t_i}) is feasible if its distances from each of the other turbines is greater than five times its diameter,

$$c_1(\mathbb{T}) = 5D - \sqrt{(x_{t_i} - x_{t_j})^2 + (y_{t_i} - y_{t_j})^2} \leq 0, \qquad \forall j \tag{8}$$

where D is the diameter of turbine i.

The regulatory constraints disallow placement of turbines in proximity with human dwellings, natural habitats, and infrastructure. We define the areas that turbines are forbidden to be placed as non-feasible areas of the domain. We assume that all the non-feasible areas of the domain can be modeled as convex polygons.

There are several well-known approaches in the literature to determine if a point is inside a polygon [53–55]; however, they are not convenient for this application because they include many conditionals and/or inverse trigonometric functions. In this study, we used an approach based the area of the non-feasible polygon. All the non-feasible polygons are considered to be convex and the non-convex polygons are divided into multiple convex polygons. The main idea is to draw lines from the location of a turbine to the vertices of the polygon, such that each adjacent pair of vertices creates a triangle with the location of turbine. The summation of the areas of these triangles is compared to the area of the polygon and if they are the same, the turbine is inside the non-feasible polygon. Thus, turbine i with coordinates (x_{t_i}, y_{t_i}) is feasible if for any non-feasible polygon called P_k,

$$c_2(\mathbb{T}) = A_{P_k} - A_{i_k} < 0, \qquad \forall k \tag{9}$$

where A_{P_k} and A_{i_k} are the area of the non-feasible polygon and the summation of the areas of the aforementioned triangles, respectively. A_{P_k} and A_{i_k} are calculated in Eq. 10 and Eq. 11 using the so-called shoelace formula [56],

$$\begin{aligned} A_{P_k} = \frac{1}{2}\left[\sum_{j=1}^{n} |(x_{v_j} y_{v_{j+1}} - y_{v_j} x_{v_{j+1}})|\right] \\ + \frac{1}{2}|(x_{v_n} y_{v_1} - y_{v_n} x_{v_1})| \end{aligned} \tag{10}$$

$$\begin{aligned} A_{i_k} = \frac{1}{2}\sum_{j=1}^{n} &|x_{t_i}(y_{v_j} - y_{v_{j+1}}) + x_{v_j}(y_{v_{j+1}} - y_{t_i}) \\ &+ x_{v_{j+1}}(y_{t_i} - y_{v_j})| + \frac{1}{2}|x_{t_i}(y_{v_n} - y_{v_1}) + x_{v_n}(y_{v_1} - y_{t_i}) \\ &+ x_{v_1}(y_{t_i} - y_{v_n})| \end{aligned} \tag{11}$$

where $j \in \{1, 2, \cdots, n\}$, n is the number of the non-feasible polygon's vertices and (x_{v_j}, y_{v_j}) are the coordinates of each vertex.

3. Multi-Objective Optimization with NSGA-II

A general multi-objective minimization problem can be formulated as,

$$\begin{aligned} &\underset{\mathbf{x}}{\text{minimize}} \quad f_1(\mathbf{x}),\ f_2(\mathbf{x}),\ \cdots,\ f_n(\mathbf{x}) \\ &\text{subject to} \quad c_i(\mathbf{x}) \leq 0, \qquad i = 1, \cdots, m \end{aligned} \tag{12}$$

where $\mathbf{x} = [x_1, x_2, \cdots, x_l]$ and n, l, and m are the cardinalities of objective functions, variables, and constraints, respectively. For a multi-objective minimization problem, it is unlikely that a solution can minimize all the objective functions simultaneously. In this case, there exists a solution set for which none of the objective functions can be improved without degrading the value of another. This set of optimal solutions is called non-dominated solution set (Pareto set).

As details of the NSGA-II genetic algorithm for unconstrained, multi-objective optimization problems can be found elsewhere (e.g., [34]), here we focus on the key non-domination sorting operation, which is based on two different metrics, non-domination rank and crowding distance. Non-domination ranking aggregates multiple objective values for each solution into a single rank indicator for each subset of the population that can be considered as equally desirable. To this end, an integer rank (starting at 1) is assigned to the non-dominated solutions. At any given rank level j, the rank-j solutions are found by searching for the non-dominated solution set after removing all the k-ranked solutions, $k = 1, \ldots, j-1$, from consideration. Crowding distance, on the other hand, is used to preserve diversity in the population and improve convergence. For a given solution, its crowding distance is calculated as its distance to the closest solution with the same rank. To discriminate between competing solutions, NSGA-II uses the non-domination rank as the primary objective and prefers solutions with greater crowding distance to break ties. In the case of a double tie, when solutions have same non-domination rank and crowding distance, both solutions are considered equally desirable.

4. Constraint Handling

In this section, we discuss the two approaches used to handle the constraints: dynamic penalty functions and hybridization of CP with the dynamic penalty approach that we call Constraint Handling via Constraint Programming (CHCP).

4.1. Penalty Functions Approach

Dynamic penalty functions [29] penalize the objective functions of the infeasible solutions with penalty coefficients that increase as the optimization process advances. The penalized objective functions using dynamic penalty approach can be formulated as,

$$\begin{aligned} f_1^P(\mathbf{x}) &= f_1(\mathbf{x}) + \sum_{i=1}^{m} (\max(0, g_i(\mathbf{x})))^2 \left(\frac{t}{n_{gen}}\right)^2 R_{f_1,i} \\ f_2^P(\mathbf{x}) &= f_2(\mathbf{x}) + \sum_{i=1}^{m} (\max(0, g_i(\mathbf{x})))^2 \left(\frac{t}{n_{gen}}\right)^2 R_{f_2,i} \\ &\vdots \\ f_n^P(\mathbf{x}) &= f_n(\mathbf{x}) + \sum_{i=1}^{m} (\max(0, g_i(\mathbf{x})))^2 \left(\frac{t}{n_{gen}}\right)^2 R_{f_n,i} \end{aligned} \tag{13}$$

where $f_1^P, f_2^P, \cdots, f_n^P$ are the penalized objective functions, $R_{f_1,i}, R_{f_2,i}, \cdots, R_{f_n,i}$ are the penalty coefficients for constraint i and different objective functions, t is the current generation number and n_{gen} is the total number of generations according to the termination criterion. In Eq. 13, the term that depends on the current generation number is squared following [57].

If we assume the proximity constraint as the first constraint, g_1 is the first constraint function and shows the amount of proximity constraint violation. This function can be defined as

$$g_1 = \sum_{i=1}^{n_T-1} \sum_{j=i+1}^{n_T} \max\left(0, 5D - \sqrt{\left(x_{t_i} - x_{t_j}\right)^2 + \left(y_{t_i} - y_{t_j}\right)^2}\right), \tag{14}$$

where n_T is the number of turbines and $\{(x_{t_i}, y_{t_i}), (x_{t_j}, y_{t_j})\}$ are the coordinates of each pair of turbines that violate the proximity constraint.

In a similar fashion to the proximity constraint, we can assume the regulatory constraint as the second constraint and calculate g_2 as the amount of regulatory constraint violation, defined as the summation of the minimum distances of the infeasible turbines to the sides of the non-feasible areas in which they are located. Hence, for a polygon with n sides the distance of turbine i from side j can be defined as the height of the triangle formed by the turbine's location point and two vertices of side j. We calculate this height by dividing the area of the triangle by the base of the triangle, i.e., side j,

$$d_{i,j} = \frac{|x_{t_i}(y_{v_j} - y_{v_{j+1}}) + x_{v_j}(y_{v_{j+1}} - y_{t_i}) + x_{v_{j+1}}(y_{t_i} - y_{v_j})|}{\sqrt{(x_{v_j} - x_{v_{j+1}})^2 + (y_{v_j} - y_{v_{j+1}})^2}} \tag{15}$$

where $j \in \{1, 2, \cdots, n\}$. Finally, g_2 can be defined as,

$$g_2 = \sum_{i=1}^{n_{reg}} \min\{d_{i,1}, d_{i,2}, \cdots, d_{i,n}\} \tag{16}$$

where n_{reg} is the number of turbines that violate the regulatory constraint.

The penalized objective functions are defined as,

$$AEP^P(\mathbb{T}) = AEP(\mathbb{T}) + \sum_{i=1}^{2} (\max(0, g_i))^2 \left(\frac{t}{n_{gen}}\right)^2 R_{AEP,i} \tag{17}$$

and

$$\begin{aligned} SPL^P(\mathbb{T}, \mathbb{R}) &= SPL(\mathbb{T}, \mathbb{R}) \\ &\quad + \sum_{i=1}^{2} (\max(0, g_i))^2 \left(\frac{t}{n_{gen}}\right)^2 R_{SPL,i}, \end{aligned} \tag{18}$$

As an infeasible solution is penalized by the dynamic penalty approach, its chance to participate in the parent selection and recombination process decreases significantly. Thus, this infeasible solution is typically discarded by the GA and a new solution is generated in the next generation. As the cardinality of feasible solutions is significantly lower in highly constrained problems, using dynamic penalty function may result in a Pareto set with a low cardinality and/or diversity [29].

4.2. Constraint Handling via Constraint Programming (CHCP)

In this study, the CHCP approach introduced in our previous work [51] is expanded to be applicable to general optimization problems. The idea behind the CP model used in the CHCP approach is to find feasible solutions that are as close as possible to the corresponding infeasible solutions in the variable space. Since this model only searches the neighborhood of the infeasible solutions, its behavior is one of local exploration, as defined in Sec. 1. The rationale and main advantage of repairing the infeasible solutions is that the GA does not have to search for new feasible solutions, which potentially reduces computational cost in highly constrained spaces [58]. In addition, repairing infeasible solutions helps explore the boundary of the feasible region, making the CP model suitable for constrained problems, for which the optimal solutions exist at the boundary of the feasible space. However, the drawback of repairing the infeasible solutions is that it reduces the global exploration behavior, which may be desirable in some cases. Our proposed CHCP balances both local and global exploration behaviors by hybridizing the CP model with penalty functions. When an infeasible solution is generated, it is first handled by the CP model. If the CP model cannot repair the solution, i.e., cannot find a feasible solution which is close enough to the infeasible solution in a certain amount of time, the infeasible solution is penalized by the dynamic penalty approach.

The CP model of the proposed CHCP approach is formulated as,

$$\begin{aligned} \underset{\mathbf{x}}{\text{minimize}} \quad & \sum_{j=1}^{l} \left(x_j^* - x_j\right)^2 \\ \text{subject to} \quad & c_i(\mathbf{x}) \leq 0, \qquad i = 1, \cdots, m \end{aligned} \tag{19}$$

where x_j^* is the value of variable x_j in the infeasible solution under repair. The objective function is the sum of squared Euclidean distances between the repaired solution and the current infeasible solution. The constraints for this subproblem are the same as those of the original optimization problem solved by the GA (i.e., Constraints 8 and 9). Since it is common to use integer variables in commercially available CP solvers (in this work we use IBM ILOG CP Optimizer V12.6 [59]), as a matter of convenience, but without loss of generality, the domains of the optimization (input) variables are discretized solely for the purpose solving this subproblem.

The CP subproblem, has three independent parameters, namely (a) the discretization resolution used for the optimization variables, (b) the computation budget (e.g. time) allocated to solving the subproblem, and (c) the maximum acceptable value of the objective function of the CP subproblem. For simplicity, hereafter we call this parameter *maximum distance*. This parameter effectively determines the size of the neighborhood that is explored during the CP subproblem. An important measure of the CHCP approach, which depends on the above mentioned parameters, is the percentage of infeasible solutions that are repaired by the CP model. Hereafter, we will refer to this quantity as *CP percentage*.

A set of preliminary experiments with different benchmark problems were conducted to evaluate the effects of the above mentioned parameters on the CP percentage [51, 58]. Based on these experiments, the domain of each variable is discretized to 150 bins. Our experiments showed that a finer discretization increases the computational cost, while CP percentage and optimization results do not change significantly. The time limit per call for the CP model is set to 10 seconds. Increasing the time limit increases the computational cost, while it does not affect CP percentage and optimization results. However, it was shown that maximum distance has a significant effect on the CP percentage and optimization results. Thus, in our experiments, the maximum distance is set to different values, while keeping the other parameters fixed.

The above mentioned CP model of the CHCP approach can be formulated for the WFLO problem as,

$$\begin{aligned}
&\underset{(x_{t_i},y_{t_i})}{\text{minimize}} \quad \sum_{i=1}^{n_{nf}} \left(\left(x^*_{t_i} - x_{t_i}\right)^2 + \left(y^*_{t_i} - y_{t_i}\right)^2 \right), \\
&\text{subject to} \quad \sqrt{(x^*_{t_j} - x_{t_i})^2 + (y^*_{t_j} - y_{t_i})^2} \geq 5D, \\
&\qquad\qquad\quad \forall j \in \{1, 2, \cdots, n_T\}, j \neq i, \\
&\qquad\qquad\quad A_{i_k} - A_{P_k} > 0 \quad \forall P_k \in \mathbb{S},
\end{aligned} \tag{20}$$

where n_{nf} is the number of infeasible turbines in an infeasible layout (i.e., the number of turbines that violate either the proximity or the regulatory constraint in an infeasible layout), $\mathbb{S}$ is the set of all the non-feasible polygons, and $(x^*_{t_i}, y^*_{t_i})$ and (x_{t_i}, y_{t_i}) are the current and repaired coordinates of the ith infeasible turbine respectively.

5. WFLO Test Cases

Tests are performed with an in-house C++ implementation of the NSGA-II algorithm and the CHCP approach uses the C++ interface of IBM ILOG CP Optimizer V12.6 [59] for the CP model. The code is compiled with the TDM-GCC version 4.7.1 compiler under Linux Red Hat version 6.2 and is run serially on a Dell PowerEdge T420 Tower Server with 2 Intel Xeon E5-2400 processors and 164 GB of RAM.

As described in [46, 50, 51], random wind farm test cases are generated with predefined feasibility percentages, as follows. Following the standard test cases in the literature, a domain of 3 km $\times$ 3 km square is considered for the wind farm. The feasibility percentage of a wind farm domain is the percentage of area available for turbine placement. This percentage is shown as ϕ from now on. The domain is divided 225 random convex polygons with similar areas. Some of these polygons are then labeled as non-feasible until the desired feasibility percentage (ϕ) is achieved.

Based on industrial wind farm design experience, nine wind farm maps with ϕ = 70%, 80%, and 90% feasibility percentages (ϕ), and 5, 10, and 15 turbines ($n_T = 5, 10,$ and 15) are considered. Figure 2 shows the map of WFLO test case with ϕ = 80% and $n_T = 10$. Shaded polygons are non-feasible. A noise receptor (indicated with a cross) is located randomly inside each non-feasible polygon. Thus, highly constrained domains contain more noise receptors.

The population size and the number of generations for the GA are set based on a set of preliminary computational experiments. For $\phi = 70\%$, a population size of 200 results in the best solutions, regardless of the number of turbines. Similarly, for $\phi = 80\%$ and 90% the population sizes of 150 and 100 perform the best, respectively.

Based on these population sizes, the corresponding number of generations is set to keep the number of objective function evaluations constant.

We followed Deb et al. [34] to set the NSGA-II parameters. The recombination and mutation probabilities are set to 0.95 and 0.05 respectively. Convergence of the optimization is determined by monitoring the changes in crowding distance for a certain number of generations. Based on our numerical experiments with a set of benchmark optimization problems from the literature [34, 36], we consider the optimization run to have converged if the variance of the crowding distance of solutions with rank 1 is less than 0.005 in the last 100 generations. In order to make the total run-time insensitive to the hardware, we set a limit of $80,000$ objective function evaluations as a termination criterion.

To account for the impact of randomness and the dependence of the penalty approach on problem-specific penalty coefficients, 20 different random seeds and two different penalty coefficients, i.e., 40 runs, are used to solve each WFLO problem (e.g. 10 turbines and 70% feasibility). The experiments for the WFLO problem are conducted with different maximum distances for the CP model and hence different CP percentages. The 40 Pareto fronts that result from these experiments for each maximum distance are merged and an overall Pareto front is determined, containing the non-dominated solutions across all 40 runs. In this work, we have favoured this approach to study the performance of the algorithms, as opposed to obtaining an average or median Pareto front across all runs, given that such definitions are not straight forward to implement and interpret in multi-dimensional spaces [60]. More specifically, using an average Pareto front, however calculated, would result in analyzing solutions that are the result of arbitrary operations in the objective space, but that may not correspond to any feasible solution in the input space.

6. Results and Discussion

In this section, we analyze the performance of the proposed CHCP approach in the constrained WFLO problem. First, we characterize the behavior of CHCP through a parametric study of the maximum acceptable value of the objective function for the CP subproblem (maximum distance), and the number of infeasible solutions generated during the optimization, in response to changes in the maximum distance, number of turbines (i.e. problem size), and land availability (constraint severity). Second, we compare the performance of CHCP with dynamic penalty functions and discuss the implications of the results for wind farm design practice. Finally, we present our results in terms of CHCP's ability to converge and computational cost for this problem.

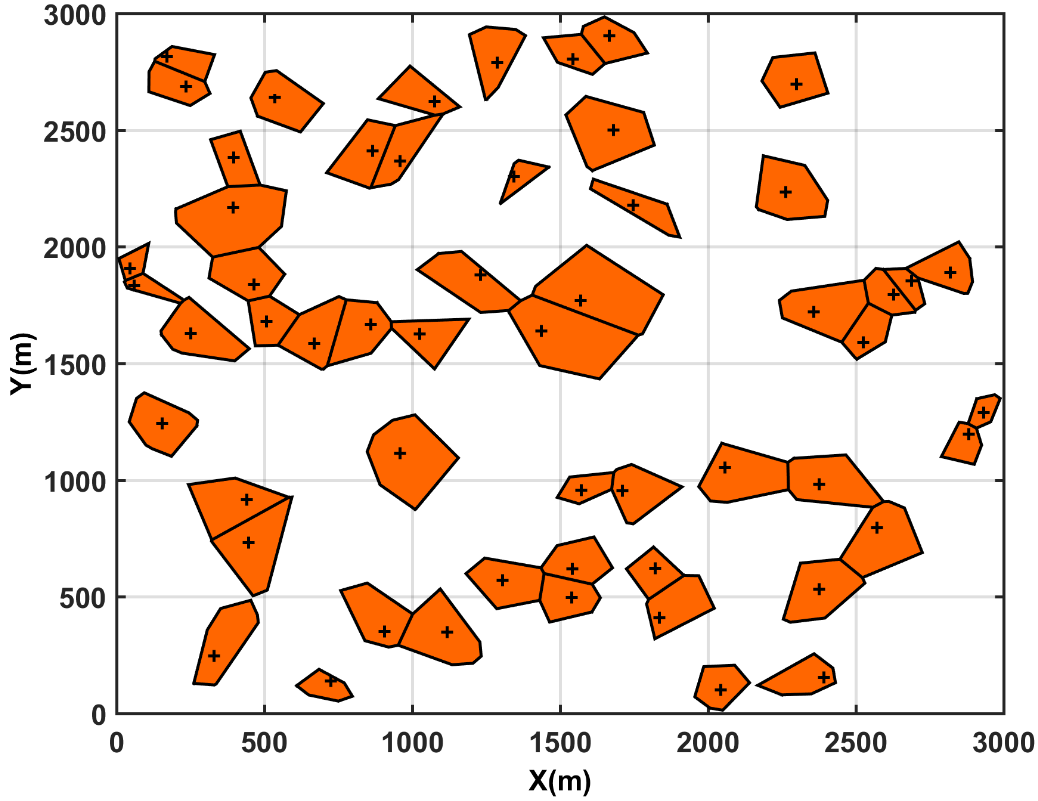

Figure 2: Sample wind farm domain. Darker areas indicate regions where turbines cannot be located. The marker (+) inside each region represents a noise receptor.

6.1. CHCP behavior

The variation of the CP percentage with different maximum distances are compared for different number of turbines in Fig. 3. Each scatter point shows the CP percentage of a test case for a specific maximum distance. It is observed that decreasing the maximum distance decreases the CP percentage. As the maximum distance decreases, the CP model is forced to find feasible solutions closer to the infeasible solutions in the same time limit. When the CP model is unable to do so, it passes these solutions to the dynamic penalty operator, thus decreasing the percentage of solutions that are effectively handled by the CP subproblem (CP percentage).

The performance of the CHCP approach on the constrained WFLO problem is evaluated in Tables 4 and 5. Table 4 compares the average number of infeasible solutions generated in 40 runs using different constraint handling approaches. For 5 and 10 turbines, using the CHCP approach results in the generation of more infea-

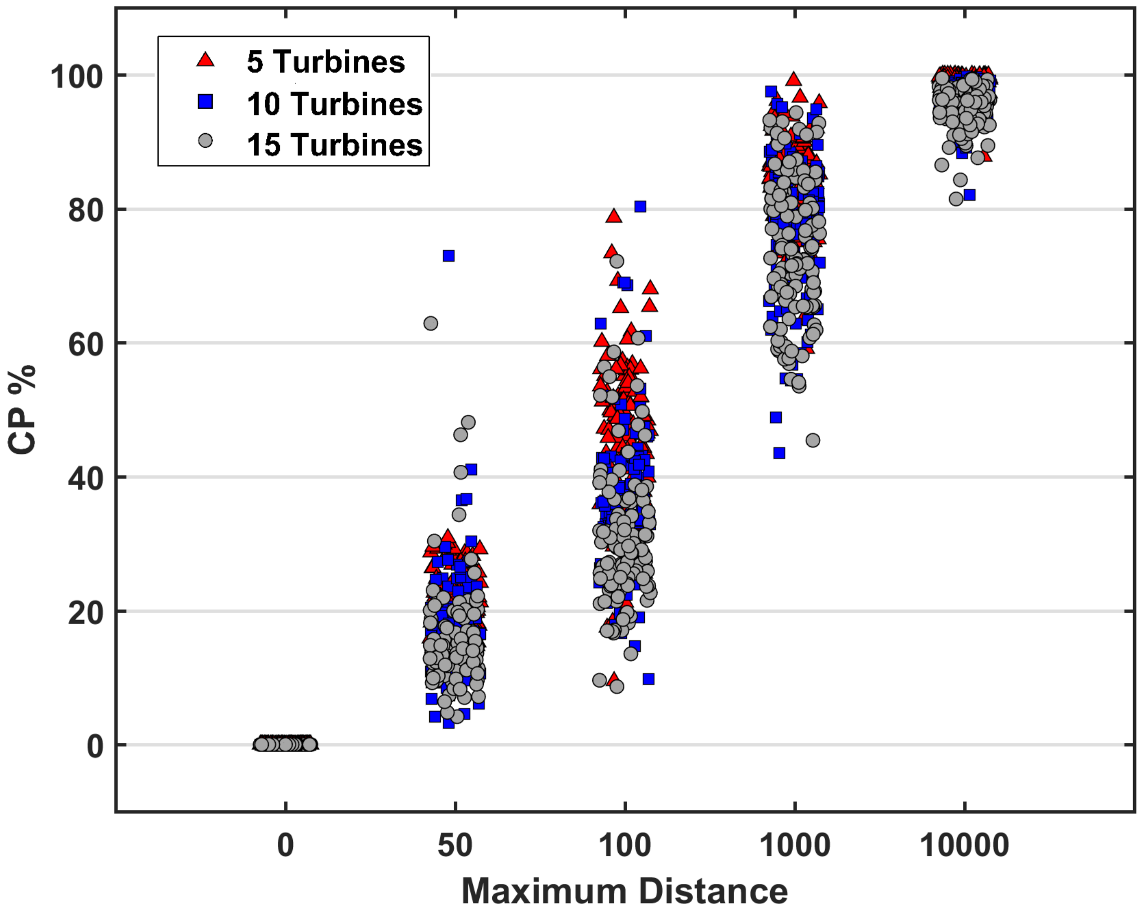

Figure 3: CP percentage for different maximum distances and different number of turbines with all the feasibility percentages (dynamic penalty is represented with a maximum distance of 0).

Table 4: Average number of infeasible layouts generated per each run by the different constraint handling approaches, for different WFLO test cases. Note that MD denotes the maximum distance used in the CP model of the proposed CHCP approach.

n_T	ϕ	Dynamic Penalty	CHCP			
			MD = 50	MD = 100	MD = 1,000	MD = 10,000
5	70%	2,190	5,308	5,324	4,672	**5,365**
5	80%	514	1,084	1,200	1,330	**1,475**
5	90%	139	286	325	**372**	239
10	70%	3,056	7,556	5,478	6,203	**7,578**
10	80%	1,869	4,203	**5,117**	3,459	5,080
10	90%	2,663	2,372	**3,809**	2,922	3,662
15	70%	**350,575**	7,827	8,723	6,808	7,681
15	80%	**416,098**	5,857	5,665	5,552	7,212
15	90%	**353,616**	5,028	5,450	4,935	6,625

sible solutions compared to using dynamic penalty approach. The CHCP approach replaces the infeasible solutions with the closest feasible solutions that can be found within the allotted computation budget. As a result, the repaired solutions lie close to the feasibility boundary, thus making it more likely for the GA operators to generate infeasible solutions through subsequent recombination and mutation operators. For 15 turbines, the number of infeasible solutions for the penalty approach increases significantly, while this number for the CHCP approach remains in the same order of magnitude as that of 5 and 10 turbines. As the number of turbines increases, more constraints are added to the domain and the probability of finding feasible solutions with the penalty approach decreases drastically. On the other hand, because the CHCP approach explores the boundary of the feasible space, it performs better in highly constrained domains. Thus, the CHCP has a more robust performance compared to the dynamic penalty approach from this point of view. Changes to the maximum distance do not show a general trend on the number of infeasible solutions for cases with different numbers of turbines or land availabilities.

Table 5 shows the CP percentage for different constraint handling approaches. As expected, for the same maximum distance, when the number of turbines increases, the CP percentage decreases. An increase in the number of turbines, makes the problem more constrained. Hence, finding feasible solutions that are close to the infeasible solutions becomes harder for the CP model. Note, however, that for the largest maximum distance, almost all infeasible solutions were repaired by the CHCP step. This illustrates the interplay between the maximum distance and the optimization problem itself in the resulting CP percentage.

Table 5: Average of the CP percentages of each run for different constraint handling approaches and different WFLO test cases. Note that MD denotes the maximum distance used in the CP model of the proposed CHCP approach.

n_T	ϕ	Dynamic Penalty	CHCP			
			MD = 50	MD = 100	MD = 1,000	MD = 10,000
5	70%	0.0	20.5	41.8	77.8	99.4
5	80%	0.0	22.9	47.8	85.0	99.6
5	90%	0.0	19.1	39.5	84.4	97.2
10	70%	0.0	19.4	42.3	80.1	97.7
10	80%	0.0	19.5	39.1	76.1	96.3
10	90%	0.0	11.0	26.5	69.0	94.6
15	70%	0.0	18.4	31.5	71.4	94.3
15	80%	0.0	16.2	31.8	71.7	94.2
15	90%	0.0	9.8	22.4	67.6	93.9

6.2. Energy-noise trade-off for constrained WFLO

Figures 4, 5, and 6 show the comparison of optimal Pareto sets found by different constraint handling approaches. In these figures, the horizontal axis is reversed with the purpose of locating the utopia point in the bottom left corner of each figure. Note that, for all the test cases except the test case with 10 turbines and 80% of land availability, there are CHCP setups that outperform the dynamic penalty approach.

For the test case with 10 turbines and 80% of land availability, Fig. 5(b) shows that the Pareto set found by the dynamic penalty approach is slightly better than those obtained when having a maximum distance, i.e., within the same energy generation, the noise production of the dynamic penalty approach is slightly lower than that of different CHCP setups. To investigate this issue further, Figure 7(a) shows the best Pareto fronts found by different setups of the CHCP approach (different CP percentages) and the Pareto fronts obtained in all 40 runs of the dynamic penalty approach. It can be observed that, in 38 of those 40 runs, the Pareto fronts obtained by CHCP outperform those obtained through dynamic penalties. However, there are 2 runs of the dynamic penalty approach that make the final Pareto set obtained with the dynamic penalty approach slightly better than those of the CHCP approach.

To explore the reason for these differences, the actual turbine layouts corresponding to these solutions, which corresponds to the points (AEP = 48.19 GWhr , SPL = 41.67 dBA), (AEP = 48.19 GWhr, SPL = 42.35 dBA), and (AEP = 48.19 GWhr, SPL = 43.68 dBA) in the objective space, obtained with dynamic penalty, MD = 1,000, and MD = 10,000 respectively, are plotted and compared to each other in Fig. 7(b). It is shown that the three layouts are similar with the main differences found

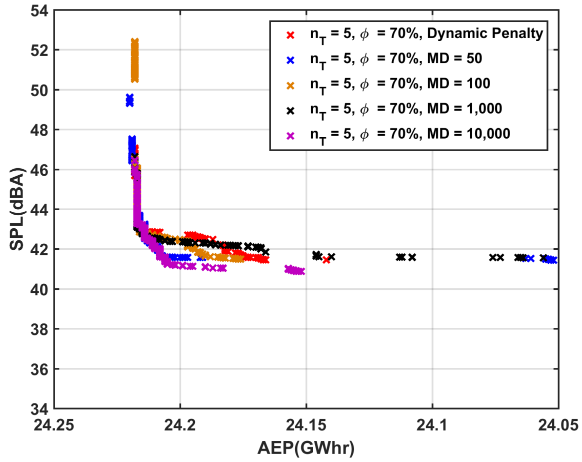

(a) $n_T = 5, \phi = 70\%$

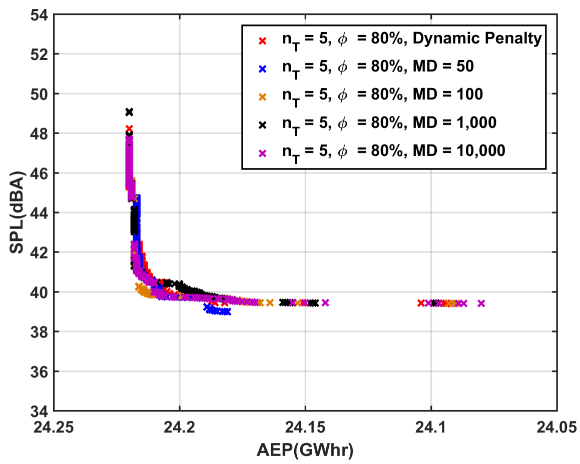

(b) $n_T = 5, \phi = 80\%$

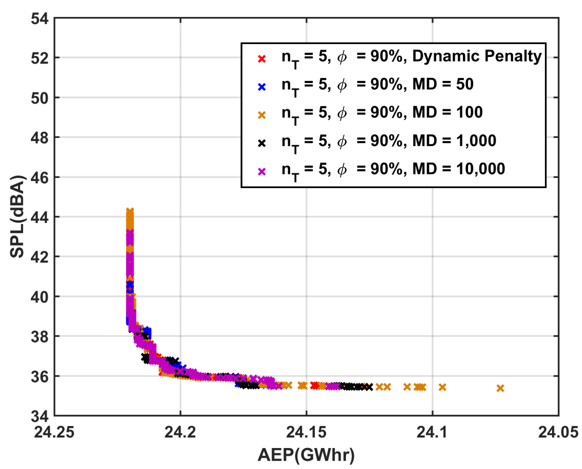

(c) $n_T = 5, \phi = 90\%$

Figure 4: Comparison of constraint handling approaches for 5 turbines (horizontal axis is reversed and ϕ shows the land availability percentage).

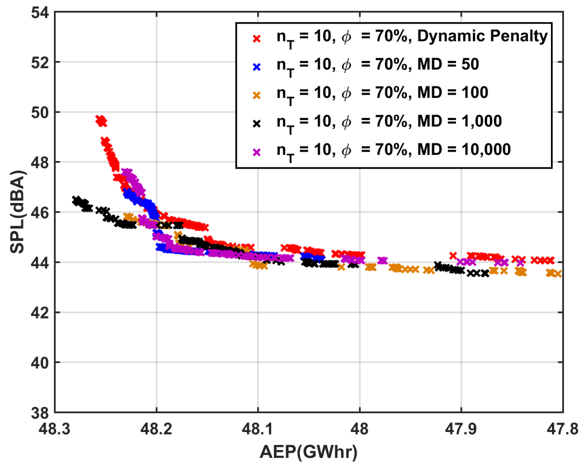

(a) $n_T = 10, \phi = 70\%$

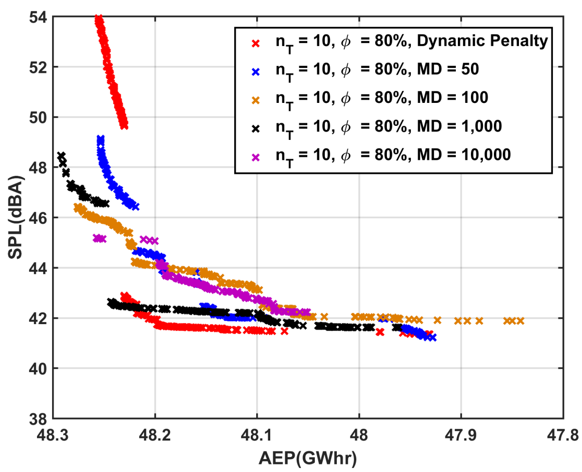

(b) $n_T = 10, \phi = 80\%$

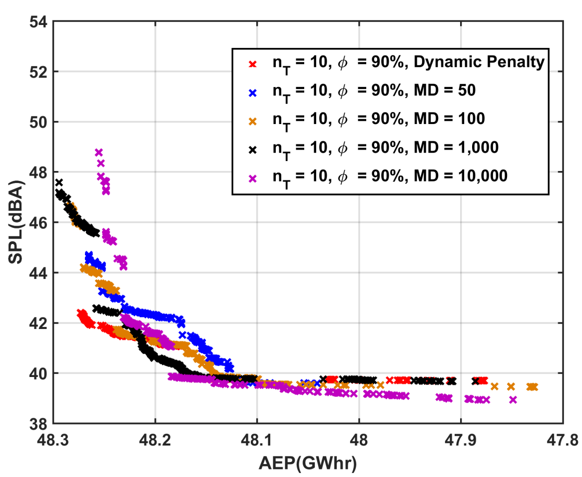

(c) $n_T = 10, \phi = 90\%$

Figure 5: Comparison of constraint handling approaches for 10 turbines (horizontal axis is reversed and ϕ shows the land availability percentage).

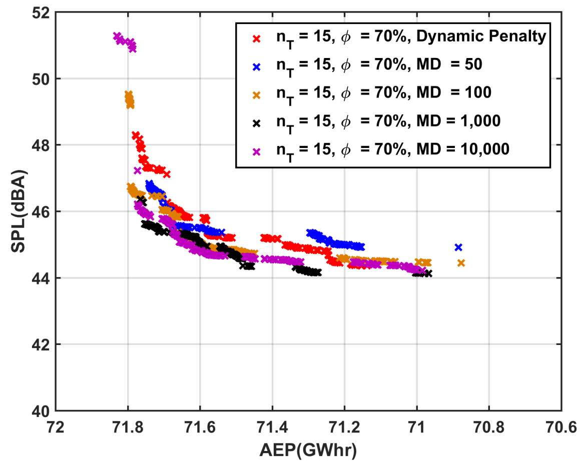

(a) $n_T = 15, \phi = 70\%$

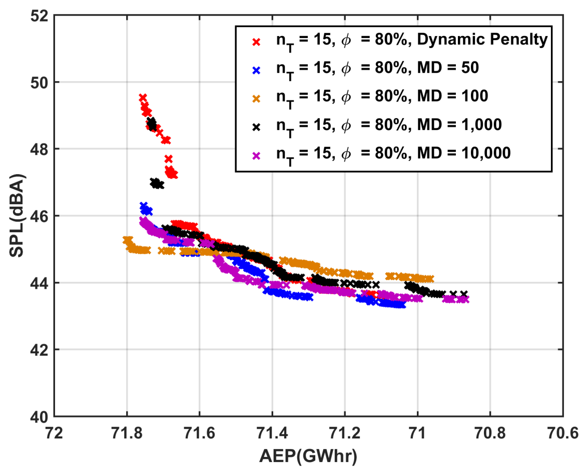

(b) $n_T = 15, \phi = 80\%$

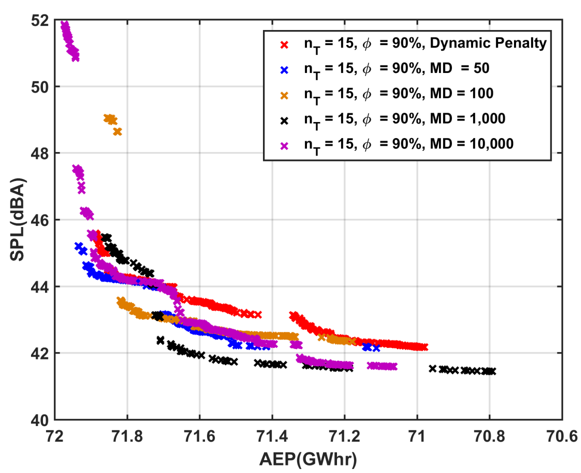

(c) $n_T = 15, \phi = 90\%$

Figure 6: Comparison of constraint handling approaches for 15 turbines (horizontal axis is reversed and ϕ shows the land availability percentage).

in the turbines residing in $Y \simeq 3000$ and $2000 < X < 3000$ for dynamic penalty case. This part of the domain is far from the non-feasible areas, which means that optimization variables with values corresponding to these coordinates would be far from the boundary of the feasible domain. Hence, the CHCP approach did not explore this area to the extent that the dynamic penalty approach did.

To study the effect of number of turbines and land availability on energy gener-

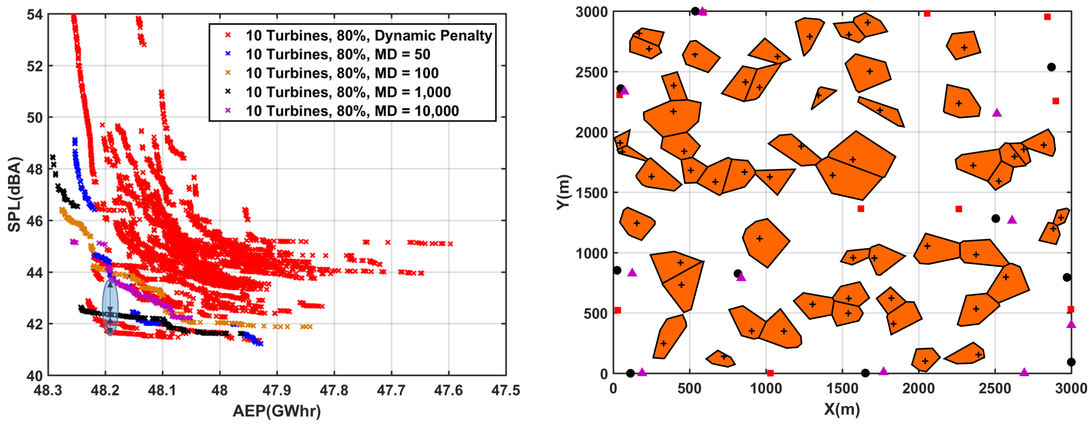

(a) Solution comparison

(b) Layout comparison

Figure 7: Comparison of the all solutions found by the dynamic penalty approach in 40 runs with the Pareto fronts of the different setups of CHCP approach and Layout comparison for Dynamic Penalty (red squares), MD = 1,000 (black circles), and MD = 10,000 (purple triangles) with same energy generation and different noise production.

ation and noise production, the best performing maximum distances are compared to study the effect of number of turbines and land availability on energy generation and noise production. Figure 8(a) compares the Pareto set of the best performing maximum distance for 15 turbines and different levels of land availability. It is shown that, as the land availability increases, energy generation is increased and noise levels at the receptors are decreased. Similarly, Fig. 8(b) compares the Pareto of the best performing maximum distance for 70% land availability and different number of turbines. As the number of turbines increases, energy generation increases significantly. However, it is possible to find layouts that have relatively the same level of noise production specially when comparing 10 turbines and 15 turbines Pareto fronts. This discussion on the results shown in Fig. 8 is in line with previous discussions published in the literature, readers are referred to [46, 50] for more details.

As the final point in our energy-noise trade-off discussion, optimization result for the test case with 15 turbines, 70 percent land availability, and using CHCP with

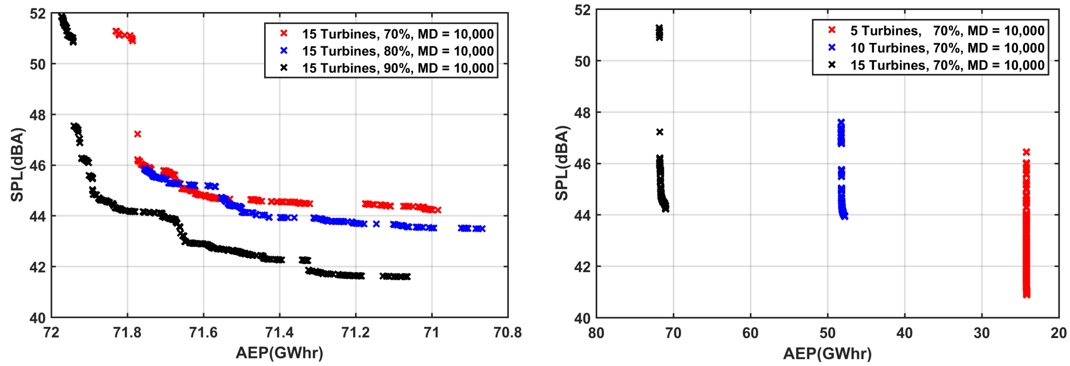

(a) 15 turbines and different land availabilities. (b) $\phi = 70\%$ and different number of turbines

Figure 8: Comparison of the best performing CP percentage for (a) 15 turbines and different land availabilities and (b) 70% land availability and different number of turbines.

MD = 10,000 are shown in Fig. 9. In this figure, the wind farm domain has been discretized into 100 m $\times$ 100 m square cells, and each square has been colored based on the number of turbines in all Pareto optimal layouts that have fallen into each cell, divided by the maximum number of turbines that any cell received. Thus, darker cells indicate that more turbines were located in this region among all the layouts in the final Pareto set. Overall, Fig. 9 is a way to visually represent a summary of all Pareto-optimal layouts, illustrating which regions of the wind farm domain are correlated with a higher probability of Pareto optimality. Of course, each Pareto-optimal layout could be visualized individually, though they are not show them here for the sake of brevity.

6.3. Convergence and computational cost

Tables 6 and 7 show the computational cost and convergence of the different constraint handling approaches for the WFLO problem. Table 6 provides evidence that the CHCP approach has lower run-times than the penalty approach. In addition, the CHCP approach results in better convergence, as suggested in Table 7 by the number of runs that met the convergence criterion set forth in Section 5. Note also that the run-time and convergence behavior of the CHCP does not have a defined trend with respect to the maximum distance.

In summary, our results show that the CHCP approach has a better overall performance compared to penalty functions when applied to constrained, multi-objective WFLO problem studied. The implementation of CHCP approach increased annual

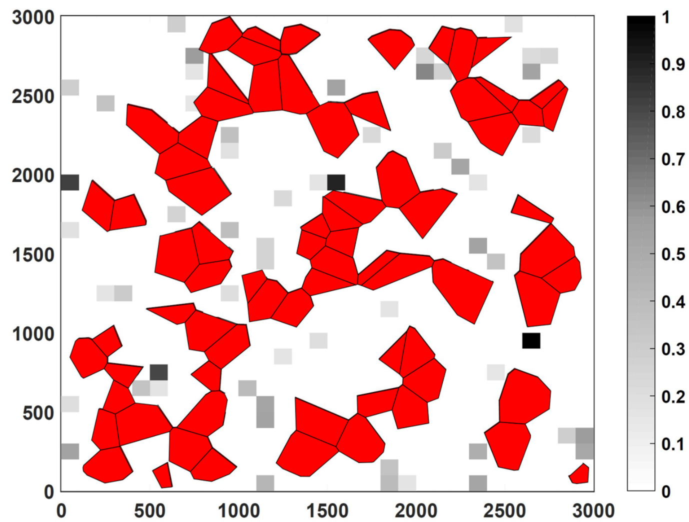

Figure 9: Final optimization result for 15 turbines, 70 percent land availability, and using CHCP with MD = 10,000.

energy generation of wind farm by a minimum value of 50 MWh for the most constrained case, while reducing the noise received by the noise receptors 0.42 dBA. This improvement is achieved while the computational cost of this approach is similar to the previous approaches.

The parameters of the CHCP approach can be tuned in such a way that its performance is optimized. The most important characteristic of the proposed CHCP approach is the maximum distance. There is a certain maximum distance for each of the investigated problems for which the proposed CHCP approach performs the best. This maximum distance varies for different problems, though it was observed that more often higher maximum distances were preferable.

7. Conclusion

In this study, the multi-objective, constrained wind farm layout optimization (WFLO) problem was solved with a novel constraint handling approach. The energy generation was maximized and the noise received by the stakeholders was minimized, while land use constraints were satisfied.

The novel constraint handling approach, Constraint Handling via Constraint Programming (CHCP) was used with Genetic Algorithms to improve optimization efficiency. This approach used a Constraint Programming (CP) model to repair infea-

Table 6: Average run-time (hr) per each run by the different constraint handling approaches, for different WFLO test cases. Note that MD denotes the maximum distance used in the CP model of the proposed CHCP approach.

n_T	ϕ	Dynamic Penalty	CHCP			
			MD = 50	MD = 100	MD = 1,000	MD = 10,000
5	70%	15.26	14.24	15.70	14.81	**13.97**
5	80%	**15.77**	17.02	17.95	16.92	16.36
5	90%	17.59	15.59	19.29	17.33	**14.56**
10	70%	55.42	48.77	**47.80**	50.03	58.93
10	80%	61.17	54.04	55.45	**54.61**	63.47
10	90%	68.56	**58.96**	60.49	63.22	66.96
15	70%	119.30	**106.85**	108.82	109.25	129.89
15	80%	124.53	117.53	**113.20**	116.53	133.04
15	90%	156.82	141.65	**138.92**	147.02	165.72

sible solutions by finding the closest feasible solutions with a given computational budget. The infeasible solutions were penalized if the CP subproblem could not be solved in the allotted time.

Solving the WFLO problem with CHCP approach resulted in finding layouts with higher energy generation, while lower noise was received by wind farm neighbors, specially for highly constrained problems. More importantly, this improvement was achieved in a lower computational time and better convergence rate compared to the previously used approaches. We expect that considering continuous variable Constraint Programming sub-problems, which might require using a different solver, such as SCIP [61] can further improve the performance of CHCP approach.

Future work on the WFLO problem could focus on expanding the proposed algorithm to consider terrain complexities such as hills. This consideration usually requires computationally expensive CFD simulations. However, the lower computational cost of the proposed approach makes it a suitable candidate for being hybridized with CFD simulations. In this case, the conditions for which the proposed CHCP approach has the best performance should be fully understood. To this end, a larger base of WFLO problems with larger number of turbines and constraints should be solved using the proposed CHCP approach.

Table 7: Number runs (out of 40 runs) that met the convergence criterion (Section 5) for different constraint handling approaches and different WFLO test cases. MD denotes the maximum distance used in the CP model of the proposed CHCP approach.

n_T	ϕ	Dynamic Penalty	CHCP			
			MD = 50	MD = 100	MD = 1,000	MD = 10,000
5	70%	16	19	17	**23**	21
5	80%	**27**	16	19	18	22
5	90%	20	24	16	25	**28**
10	70%	6	6	**12**	5	8
10	80%	8	**9**	7	7	7
10	90%	16	18	**19**	13	**19**
15	70%	0	**2**	1	1	**2**
15	80%	3	2	4	**5**	3
15	90%	5	8	**9**	4	5

Acknowledgment

This work was supported by the Natural Sciences and Engineering Research Council of Canada (NSERC), through the Collaborative Research and Development (CRD) and Discovery Grant programs. The authors would like to thank Hatch Ltd. for its financial support of this research.

References

[1] International Energy Association (IEA) Wind, 2012 Annual Report, IEA Wind (2013).

[2] Global Wind Energy Council (GWEC), Global Wind Report: Annual market update 2013, GWEC (2014).

[3] Wind in power: 2016 European statistics, Wind Europe (2017).

[4] Chief Medical Officer of Health (CMOH) of Ontario, The Potential Health Impact of Wind Turbines, Technical Report, Ministry of Health and Long-term Care, Government of Canada, 2010.

[5] Ministry of the Environment (Canada), Compliance Protocol for Wind Turbine Noise - Guideline for Acoustic Assessment and Measurement, Technical Report, Ministry of the Environment (Canada), 2011.

[6] Ministry of the Environment (Canada), Noise Guidelines for Wind Farms, Technical Report, 2008.

[7] G. Mosetti, C. Poloni, B. Diviacco, Optimization of wind turbine positioning in large windfarms by means of a genetic algorithm, Journal of Wind Engineering and Industrial Aerodynamics 51 (1994) 105–16.

[8] S. Grady, M. Hussaini, M. M. Abdullah, Placement of wind turbines using genetic algorithms, Renewable Energy 30 (2005) 259–70.

[9] S. Chowdhury, J. Zhang, A. Messac, L. Castillo, Characterizing the influence of land configuration on the optimal wind farm performance, in: ASME 2011 International Design Engineering Technical Conferences & Computers and Information in Engineering Conference (IDETC/CIE 2011), no. DETC2011-48731, ASME, 2011.

[10] L. Chen, E. MacDonald, A system-level cost-of-energy wind farm layout optimization with landowner modeling, Energy Conversion and Management 77 (2014) 484–94.

[11] L. Chen, E. MacDonald, Considering landowner participation in wind farm layout optimization, Journal of Mechanical Design 134 (2012) 084506.

[12] L. Chen, E. MacDonald, Effects of uncertain land availability, wind shear, and cost on wind farm layout, in: ASME 2013 International Design Engineering Technical Conferences and Computers and Information in Engineering Conference, American Society of Mechanical Engineers, 2013, pp. V03AT03A025–.

[13] Y. Chen, H. Li, K. Jin, Q. Song, Wind farm layout optimization using genetic algorithm with different hub height wind turbines, Energy Conversion and Management 70 (2013) 56–65.

[14] J. Y. Kuo, D. A. Romero, J. C. Beck, C. H. Amon, Wind farm layout optimization on complex terrains–integrating a cfd wake model with mixed-integer programming, Applied Energy 178 (2016) 404–14.

[15] W. Y. Kwong, P. Y. Zhang, D. A. Romero, J. Moran, M. Morgenroth, C. H. Amon, Wind farm layout optimization considering energy generation and noise propagation, in: Proc. International Design Engineering Technical Conferences & Computers and Information in Engineering Conference (IDETC/CIE12), 2012, pp. 1–10.

[16] W. Y. Kwong, P. Y. Zhang, D. A. Romero, J. Moran, M. Morgenroth, C. H. Amon, Multi-Objective Wind Farm Layout Optimization Considering Energy Generation and Noise Propagation with NSGA-II, Journal of Mechanical Design 136 (2014) 091010–1.

[17] P. Y. Zhang, D. A. Romero, J. C. Beck, C. H. Amon, Solving wind farm layout optimization with mixed integer programs and constraint programs, EURO Journal on Computational Optimization 2 (2014) 195–219.

[18] J. H. Holland, Adaptation in natural and artificial systems: An introductory analysis with applications to biology, control, and artificial intelligence., University of Michigan Press, 1975.

[19] J. Kennedy, Particle swarm optimization, in: Encyclopedia of Machine Learning, Springer, 2010, pp. 760–6.

[20] C. Wan, J. Wang, G. Yang, X. Zhang, Optimal micro-siting of wind farms by particle swarm optimization, in: Advances in swarm intelligence, Springer, 2010, pp. 198–205.

[21] M. Bilbao, E. Alba, Simulated annealing for optimization of wind farm annual profit, in: Logistics and Industrial Informatics, 2009. LINDI 2009. 2nd International, IEEE, 2009, pp. 1–5.

[22] B. L. Du Pont, J. Cagan, An extended pattern search approach to wind farm layout optimization, Journal of Mechanical Design 134 (2012) 081002.

[23] S. Donovan, G. Nates, H. Waterer, R. Archer, Mixed integer programming models for wind farm design, in: Slides used at MIP 2008 Workshop on Mixed Integer Programming, Columbia University, New York City, 2008.

[24] S. Donovan, An improved mixed integer programming model for wind farm layout optimisation, in: Proceedings of the 41th Annual Conference of the Operations Research Society, Wellington, New Zealand, 2006.

[25] P. Fagerfjäll, Optimizing wind farm layout: more bang for the buck using mixed integer linear programming, Chalmers University of Technology and Gothenburg University (2010).

[26] R. Archer, G. Nates, S. Donovan, H. Waterer, Wind turbine interference in a wind farm layout optimization mixed integer linear programming model, Wind Engineering 35 (2011) 165–75.

[27] S. Turner, D. A. Romero, P. Y. Zhang, C. H. Amon, T. C. Y. Chan, A new mathematical programming approach to optimize wind farm layouts, Renewable Energy 63 (2014) 674–80.

[28] D. Guirguis, D. A. Romero, C. H. Amon, Toward efficient optimization of wind farm layouts: Utilizing exact gradient information, Applied Energy 179 (2016) 110–23.

[29] C. A. Coello Coello, Theoretical and numerical constraint-handling techniques used with evolutionary algorithms: a survey of the state of the art, Computer methods in applied mechanics and engineering 191 (2002) 1245–87.

[30] R. Datta, M. F. P. Costa, K. Deb, A. Gaspar-Cunha, An evolutionary algorithm based pattern search approach for constrained optimization, in: Evolutionary Computation (CEC), 2013 IEEE Congress on, IEEE, 2013, pp. 1355–62.

[31] S. M. Elsayed, R. A. Sarker, D. L. Essam, Adaptive configuration of evolutionary algorithms for constrained optimization, Applied Mathematics and Computation 222 (2013) 680–711.

[32] S. Oh, C. Ahn, M. Jeon, Effective constraints based evolutionary algorithm for constrained optimization problems, International Journal of Innovative Computing, Information and Control 8 (2012) 3997–4014.

[33] C. M. Fonseca, P. J. Fleming, Multiobjective optimization and multiple constraint handling with evolutionary algorithms. I. A unified formulation, Systems, Man and Cybernetics, Part A: Systems and Humans, IEEE Transactions on 28 (1998) 26–37.

[34] K. Deb, A. Pratap, S. Agarwal, T. Meyarivan, A fast and elitist multiobjective genetic algorithm: NSGA-II, Evolutionary Computation, IEEE Transactions on 6 (2002) 182–97.

[35] T. Ray, K. Tai, K. C. Seow, Multiobjective design optimization by an evolutionary algorithm, Engineering Optimization 33 (2001) 399–424.

[36] H. Jain, K. Deb, An evolutionary many-objective optimization algorithm using reference-point based nondominated sorting approach, part II: Handling constraints and extending to an adaptive approach, Evolutionary Computation, IEEE Transactions on 18 (2014) 602–22.

[37] A. W. Mohamed, H. Z. Sabry, Constrained optimization based on modified differential evolution algorithm, Information Sciences 194 (2012) 171–208.

[38] S. Wang, J. Chen, K.-J. Wang, Resource portfolio planning of make-to-stock products using a constraint programming-based genetic algorithm, Omega 35 (2007) 237–46.

[39] S. Di Alesio, L. Briand, S. Nejati, A. Gotlieb, Combining genetic algorithms and constraint programming to support stress testing of task deadlines, ACM Transactions on Software Engineering & Methodology (2015).

[40] Y. Zhu, D. Qin, Y. Zhu, X. Cao, Genetic algorithm combination of boolean constraint programming for solving course of action optimization in influence nets, International Journal of Intelligent Systems and Applications (IJISA) 3 (2011) 1.

[41] N. O. Jensen, A note on wind generator interaction, 1983.

[42] D. J. Renkema, Validation of wind turbine wake models, Master of Science Thesis, Delft University of Technology 19 (2007).

[43] H. Dobesch, G. Kury, Basic meteorological concepts and recommendations for the exploitation of wind energy in the atmospheric boundary layer, Zentralanstalt für Meteorologie und Geodynamik, 2006.

[44] E. Djerf, H. Mattsson, Evaluation of the software program windfarm and comparisons with measured data from alsvik, The aeronautical research institute of Sweden (2000).

[45] J. S. González, A. G. G. Rodriguez, J. C. Mora, J. R. Santos, M. B. Payan, Optimization of wind farm turbines layout using an evolutive algorithm, Renewable energy 35 (2010) 1671–81.

[46] S. Yamani Douzi Sorkhabi, D. A. Romero, G. K. Yan, M. D. Gu, J. Moran, M. Morgenroth, C. H. Amon, The impact of land use constraints in multi-objective energy-noise wind farm layout optimization, Renewable Energy 85 (2016) 359–70.

[47] A. Crespo, J. Hernandez, S. Frandsen, Survey of modelling methods for wind turbine wakes and wind farms, Wind energy 2 (1999) 1–24.

[48] R. Shakoor, M. Y. Hassan, A. Raheem, Y.-K. Wu, Wake effect modeling: A review of wind farm layout optimization using jensen s model, Renewable and Sustainable Energy Reviews 58 (2016) 1048–59.

[49] A. Kusiak, Z. Song, Design of wind farm layout for maximum wind energy capture, Renewable Energy 35 (2010) 685–94.

[50] S. Yamani Douzi Sorkhabi, D. A. Romero, G. K. Yan, M. D. Gu, J. Moran, M. Morgenroth, C. H. Amon, Multi-objective energy-noise wind farm layout optimization under land use constraints, in: ASME 2014 International Mechanical Engineering Congress & Exposition, Manuscript Number IMECE2014-37063, 2014.

[51] S. Yamani Douzi Sorkhabi, D. A. Romero, J. C. Beck, C. H. Amon, Constrained multi-objective wind farm layout optimization: Introducing a novel constraint handling approach based on constraint programming, in: ASME 2015 International Design Engineering Technical Conferences & Computers and Information in Engineering Conference, American Society of Mechanical Engineers, 2015.

[52] ISO 9613-2:1996, Acoustics - Attenuation of sound during propagation outdoors - Part 2: General method of calculation (ISO 9613-2:1996), ISO, Geneva, Switzerland, 1996.

[53] M. Shimrat, Algorithm 112: position of point relative to polygon, Communications of the ACM 5 (1962) 434.

[54] S. G. Krantz, S. Kress, R. Kress, Handbook of complex variables, Springer, 1999.

[55] A. Van Dam, S. K. Feiner, M. McGuire, D. F. Sklar, Computer graphics: principles and practice, Pearson Education, 2013.

[56] D. Zwillinger, CRC standard mathematical tables and formulae, CRC press, 1987.

[57] J. A. Joines, C. R. Houck, On the use of non-stationary penalty functions to solve nonlinear constrained optimization problems with GA's, in: Evolutionary Computation, 1994. IEEE World Congress on Computational Intelligence., Proceedings of the First IEEE Conference on, IEEE, 1994, pp. 579–84.

[58] S. Yamani Douzi Sorkhabi, Multi-objective energy-noise wind farm layout optimization under land use constraints, 2015.

[59] IBM, ILOG, ILOG CPLEX Optimization Studio V12.6, 2013.

[60] G. Aloupis, Geometric measures of data depth, DIMACS Series in Discrete Mathematics and Theoretical Computer Science 72 (2006) 147.

[61] Zuse Institute Berlin (ZIB), SCIP Optimization Suite V3.1.1, 2015.